A conserved mediator hinge revealed in the structure of the MED7·MED21 (Med7·Srb7) heterodimer

Sonja Baumli, Sabine Hoeppner, Patrick Cramer

Angaben zur Veröffentlichung / Publication details:

Baumli, Sonja, Sabine Hoeppner, and Patrick Cramer. 2005. "A conserved mediator hinge revealed in the structure of the MED7·MED21 (Med7·Srb7) heterodimer." *Journal of Biological Chemistry* 280 (18): 18171–78. https://doi.org/10.1074/jbc.m413466200.

THE JOURNAL OF BIOLOGICAL CHEMISTRY
Vol. 280, No. 18, Issue of May 6, pp. 18171–18178, 2005
Printed in U.S.A.

A Conserved Mediator Hinge Revealed in the Structure of the MED7·MED21 (Med7·Srb7) Heterodimer*

Received for publication, November 30, 2004, and in revised form, January 18, 2005
Published, JBC Papers in Press, February 14, 2005, DOI 10.1074/jbc.M413466200

Sonja Baumli, Sabine Hoeppner, and Patrick Cramer‡

From the Gene Center, University of Munich (Ludwig-Maximilians-Universität), Department of Chemistry and Biochemistry, Feodor-Lynen-Strasse 25, 81377 Munich, Germany

The Mediator of transcriptional regulation is the central coactivator that enables a response of RNA polymerase II (Pol II) to activators and repressors. We present the 3.0-Å crystal structure of a highly conserved part of the Mediator, the MED7·MED21 (Med7·Srb7) heterodimer. The structure is very extended, spanning one-third of the Mediator length and almost the diameter of Pol II. It shows a four-helix bundle domain and a coiled-coil protrusion connected by a flexible hinge. Four putative protein binding sites on the surface allow for assembly of the Mediator middle module and for binding of the conserved subunit MED6, which is shown to bridge to the Mediator head module. A flexible MED6 bridge and the MED7·MED21 hinge could account for changes in overall Mediator structure upon binding to Pol II or activators. Our results support the idea that transcription regulation involves conformational changes within the general machinery.

Regulation of eukaryotic mRNA transcription requires multiprotein coactivators, which transmit signals from gene-specific transcription factors to Pol II[1] (1). Over the last decade, evidence from many laboratories converged on the Mediator complex as a central Pol II coactivator (2–4). Mediator was discovered in the yeast *Saccharomyces cerevisiae* by its ability to enable activated transcription in an *in vitro* system containing Pol II and the general transcription factors (5–7). Genome-wide studies showed that Mediator is required for regulated transcription of the majority of yeast genes (8). Mediator also stimulates basal transcription (9, 10). The yeast Mediator comprises 25 polypeptide subunits, of which 11 are essential and 22 are at least partially conserved in sequence throughout eukaryotes (11, 12). Nine of the Mediator subunits are products of the *srb* genes, which were discovered in a genetic screen for suppressors of truncations of the C-terminal domain of the largest Pol II subunit (13, 14). Four of the Srb proteins reside in an independent Cdk-cyclin subcomplex that is only found in a subpopulation of Mediator complexes.

Mediator promotes initiation complex assembly through activator-Mediator, Mediator-Pol II, and Mediator-general transcription factor contacts (15). Mediator also stimulates the kinase activity of the general transcription factor TFIIH, which phosphorylates the Pol II C-terminal domain, apparently triggering the transition from transcription initiation to elongation (6). Mediator is recruited to active genes ahead of Pol II (16) and is thought to remain near the promoter to facilitate transcription reinitiation (17, 18). Electron microscopy shows that Mediator undergoes strong structural changes upon interaction with Pol II (19–21) and with transcription activators (22) that are obvious even at 35 Å resolution (21). The causes and consequences of these changes are, however, poorly understood, and the molecular mechanism of Mediator remains enigmatic mainly because of a complete lack of detailed structural information.

The Mediator subunit architecture was inferred from biochemical, genetic, and electron microscopic studies. Biochemical studies defined three submodules of Mediator, the MED17 (Srb4), the MED9/10, and the MED15 (Gal11) submodules (23), which were tentatively correlated with three density lobes in electron microscopic images, termed the head, middle, and tail module, respectively (24). The head and middle modules form a core Mediator that can be isolated from yeast (17). Core Mediator enables 4-fold activation of transcription in nuclear extracts compared with 18-fold activation for the complete Mediator. The middle module is the most conserved part of Mediator and comprises subunits MED7, MED21, MED10, MED1, MED4, MED9, and possibly MED31. With the exception of MED31 (Soh1) (25), MED7 and MED21 show the highest degree of sequence homology of all core Mediator subunits (40 and 45% between yeast and human, respectively). The high conservation of MED7 and MED21 is reflected in their essential function in yeast (26, 27) and in a requirement for MED21 in mouse development (28).

To explore the general Mediator mechanism, we have determined the structure of the highly conserved heterodimeric MED7·MED21 subcomplex in two different conformational states and have analyzed the multiple direct protein interactions of this subcomplex *in vitro*. We show that highly conserved elements confer flexibility to the Mediator complex that may be important for function.

EXPERIMENTAL PROCEDURES

Cloning—The genes of MED10His and MED4His were cloned into pET21b vector (Novagen) using the restriction sites NdeI and NotI so that a C-terminal hexahistidine tag (His) was introduced. For bicistronic expression of MED7 with MED21His, MED4 with MED21His, and MED10 with MED21His, the genes of MED7, MED4, and MED10 were cloned into the pET21b vector using the restriction sites NheI and EcoRI. The gene of MED21 was then inserted together with a second ribosomal binding site at the 5′ region of the MED21 gene as described (29). The sequence of the primer was GGACGCGTCGACAATAATTTT-

* This work is supported by the Deutsche Forschungsgemeinschaft, the Fonds der Chemischen Industrie, and the EMBO Young Investigator Programme. The costs of publication of this article were defrayed in part by the payment of page charges. This article must therefore be hereby marked "*advertisement*" in accordance with 18 U.S.C. Section 1734 solely to indicate this fact.

The atomic coordinates and structure factors (codes 1YKH and 1YKE) have been deposited in the Protein Data Bank, Research Collaboratory for Structural Bioinformatics, Rutgers University, New Brunswick, NJ (http://www.rcsb.org/).

‡ To whom correspondence should be addressed. Tel.: 49-89-2180-76951; Fax: 49-89-2180-76999; E-mail: cramer@LMB.uni-muenchen.de.

[1] The abbreviations used are: Pol II, RNA polymerase II; GST, glutathione *S*-transferase; Bicine, *N*,*N*-bis(2-hydroxyethyl)glycine; Ni-NTA, nickel nitrilotriacetic acid; MAD, multiwavelength anomalous diffraction.

GTTTAACTTTAAGAAGGAGATATACATATGACAGATAGAGATTAACACAATTGC (the start of the MED21 open reading frame is underlined). The restriction sites used were SalI and NotI. The genes for variants MED7ΔNΔC·MED21His (comprised of residues 102–205 of MED7) and MED7ΔNΔC·MED21 were cloned in the same way in the pET24b vector, which contains a kanamycin resistance cassette. For MED7ΔNΔC·MED21 the restriction site XhoI was used instead of NotI. MED7ΔNΔC·MED21ΔC (comprising residues 1–132 of MED21) was cloned in pet21b and contains methionine mutations (see x-ray structure determination). Glutathione *S*-transferase (GST)-MED17ΔN, comprising residues 241–688 of yeast MED17 and an N-terminal GST tag, was cloned into the BamHI site of pGEX-3x (Amersham Biosciences). The gene of MED6 and an additional ribosomal binding site at its 5′-region were inserted into the Xma site, fused to a C-terminal His tag. Genomic DNA was used as a template for all constructs except for MED17, where a MED17-containing plasmid was used (30). MED6His was obtained from N. Lehming (31).

Protein Expression and Purification—All proteins were expressed for 16 h at 20 °C in *Escherichia coli* BL21 DE3 (Stratagene). Heterodimeric complexes were coexpressed from a single bicistronic plasmid. For coexpression of a third protein, a second plasmid was cotransformed that contains the appropriate gene and a different antibiotic resistance (ampicillin). For protein purification, cell pellets were thawed and lysed by sonication in buffer A (150 mM NaCl, 50 mM Tris, pH 8.0, 10 mM β-mercaptoethanol). After centrifugation, the supernatant was loaded onto a Ni-NTA column (Qiagen) equilibrated with buffer A. After washing with 30 ml of buffer A, bound proteins were eluted with buffer A containing 200 mM imidazole. All complexes except MED6His·MED7ΔNΔC·MED21 and GSTMED17ΔN·MED6His were further purified by anion exchange chromatography (Mono Q, Amersham Biosciences). The column was equilibrated with buffer B (50 mM NaCl, 20 mM Tris, pH 8.0, 5 mM dithiothreitol), and the proteins were eluted with a linear gradient of 20 column volumes from 50 mM to 1 M NaCl in buffer B. After concentration, the sample was applied to a Superose-6 high resolution gel filtration column (Amersham Biosciences) equilibrated with buffer C (150 mM NaCl, 20 mM Bicine, pH 8.5, 5 mM dithiothreitol). Purification of the triple methionine mutant was as for MED7ΔNΔC·MED21His, except for the Ni-NTA purification step. Instead, the mutant was precipitated with 35% saturated ammonium sulfate solution. For crystallization, the MED7ΔNΔC·MED21His peak fraction was concentrated to 16 mg/ml. MED6His·MED7ΔNΔC·MED21 was further purified by ammonium sulfate precipitation as above followed by gel filtration as above. GSTMED17ΔN·MED6His was purified by sequential Ni-NTA and GST affinity chromatography according to the manufacturer (CL4B, Amersham Biosciences). Bands of copurified proteins were generally verified by Edman sequencing.

Crystallization and Crystal Treatment—Samples were crystallized at 20 °C with the hanging drop vapor diffusion method. Selenomethionine crystals of the triple methionine mutant of MED7ΔNΔC·MED21ΔC were crystallized using the reservoir solution 100 mM sodium potassium tartrate, 100 mM Hepes, pH 7.5, 5% polyethylene glycol 400, 10 mM β-mercaptoethanol, 10 mM EDTA. Mutant MED7ΔNΔC·MED21ΔC was crystallized in 500 mM sodium acetate, 100 mM Hepes, pH 7.5, 5% polyethylene glycol 400, 10 mM β-mercaptoethanol, and 10 mM EDTA. Crystals were harvested in mother solution, which was exchanged gradually against mother solution containing additionally 35% glycerol. Crystals were flash-cooled in liquid nitrogen. Crystals of the native and selenomethionine MED7ΔNΔC·MED21His complex were grown in 0.8–1.1 M NaCl, 10–15% ethanol, 0–3% polyethylene glycol 6000, 10 mM β-mercaptoethanol, and 10 mM EDTA. The mother solution was exchanged by the same solution containing 25% glycerol, but no ethanol, using microdialysis buttons.

X-ray Structure Determination—All diffraction data were collected at the Swiss Light Source, Villigen, Switzerland. For MAD phasing, three additional methionines were introduced at positions of conserved hydrophobic residues in MED21ΔC (L5M/L119M/L125M). Selenomethionine was incorporated as described (32). MAD experiments were performed on selenomethionine-labeled crystals, and diffraction data were processed with DENZO and SCALEPACK (33) (see Table I). Four selenium sites were correctly identified with program SOLVE (34) and refined using SHARP (35). Three additional selenium peaks were detected in residual electron density maps with SHARP. Phasing with SHARP using seven consistent peaks led to an electron density map that revealed distinct α-helices. A total of 10 methionine residues are present in the amino acid sequences and were ordered in the electron density map, except the two N-terminal methionines and Met-42 of MED21. Using the selenium sites as sequence markers, most of MED7 and MED21 could be built into the electron density map at 3.6 Å of resolution with program O (36). This initial model was repositioned in the unit cell of the native crystal by rigid body refinement with CNS (37). Model-phased maps at the final resolution of 3.0 Å allowed us to complete and refine the structure with CNS to a free R-factor of 28.9% (see Table I). The second crystal form, belonging to space group $C222_1$, was phased using the 4-helix bundle of the refined MED7·MED21 structure. A difference electron density map phased with the bundle domain showed locations of the coiled-coil protrusions in the two heterodimers of the asymmetric unit that deviated substantially from that observed in the original structure. The coiled-coil region was adjusted. An extended loop between MED21 helices α1 and α2 that was disordered in the $P4_322$ crystal form was added as polyalanine in one of two heterodimers in the asymmetric unit, and the resulting model was refined to a free R-factor of 31.4% (see Table I). The MED21 loop α1-α2 is better ordered in the $C222_1$ crystal form since it forms a crystal contact that is not observed in the $P4_322$ crystal form. In both refined structures, none of the residues fall in disallowed regions of the Ramachandran plot (see Table I).

RESULTS

Subcomplex Mapping—Individually expressed recombinant Mediator subunits are generally insoluble, explaining the current lack of Mediator subunit structures. Insolubility apparently results from a loss of structural integrity when subunits are outside their natural multiprotein context. To overcome this obstacle, we coexpressed the highly conserved and essential *S. cerevisiae* Mediator subunits MED7 and MED21 in *E. coli* with the use of a bicistronic vector (compare "Experimental Procedures"). A stable MED7·MED21 complex was purified and subjected to partial proteolysis to probe for flexible regions that may interfere with crystallization. Chymotrypsin treatment resulted in the removal of 101 poorly conserved N-terminal residues of MED7 (Fig. 1). A corresponding variant MED7ΔN (MED7 residues 102–222) still formed a stable complex with MED21 after coexpression. Proteinase K treatment of the purified MED7ΔN·MED21 complex resulted in cleavage of a short C-terminal portion of MED7. A subsequently prepared variant MED7ΔNΔC (residues 102–205) still bound MED21 strongly. This variant comprises only the highly conserved region of MED7, which shows 59% sequence homology between the yeast and human proteins. Except for a short C-terminal truncation, MED21 remained stable in all proteolysis experiments. In contrast, individually expressed MED21 was readily cleaved before residues 38 and 76 (Fig. 1*B*). Therefore, MED21 is protected from degradation upon MED7 binding. Taken together, iterative proteolysis and truncation of coexpressed and copurified subunits allowed us to map a stable subcomplex, and this approach may be used to obtain potentially crystallizable portions of other multiprotein complexes.

Structure Determination—The preparations of the MED7ΔNΔC·MED21 subcomplex were monodisperse and homogeneous according to dynamic light scattering and size exclusion chromatography. The subcomplex formed crystals that grew to a maximum size of 0.6 × 0.3 × 0.3 mm and comprise two heterodimers per asymmetric unit (space group $C222_1$). Despite the large size of the crystals, diffraction extended only to 3.3 Å in favorable cases, most likely because of the very high solvent content of 78%. To increase the resolution limit of the crystals, we truncated eight non-conserved amino acid residues from the MED21 C terminus (variant MED21ΔC, residues 1–132, Fig. 1*B*). The resulting complex MED7ΔNΔC·MED21ΔC formed crystals that adopted space group $P4_322$. These crystals were slightly more stable, and could be used for structure determination. The structure was solved with MAD data from a selenomethionine-substituted crystal and was refined to a free R-factor of 28.9% against native diffraction data extending to 3.0 Å of resolution ("Experimental Procedures," Table I). We used the refined structure of the MED7ΔNΔC·MED21ΔC heterodimer to solve the structure in the initial crystal form (space

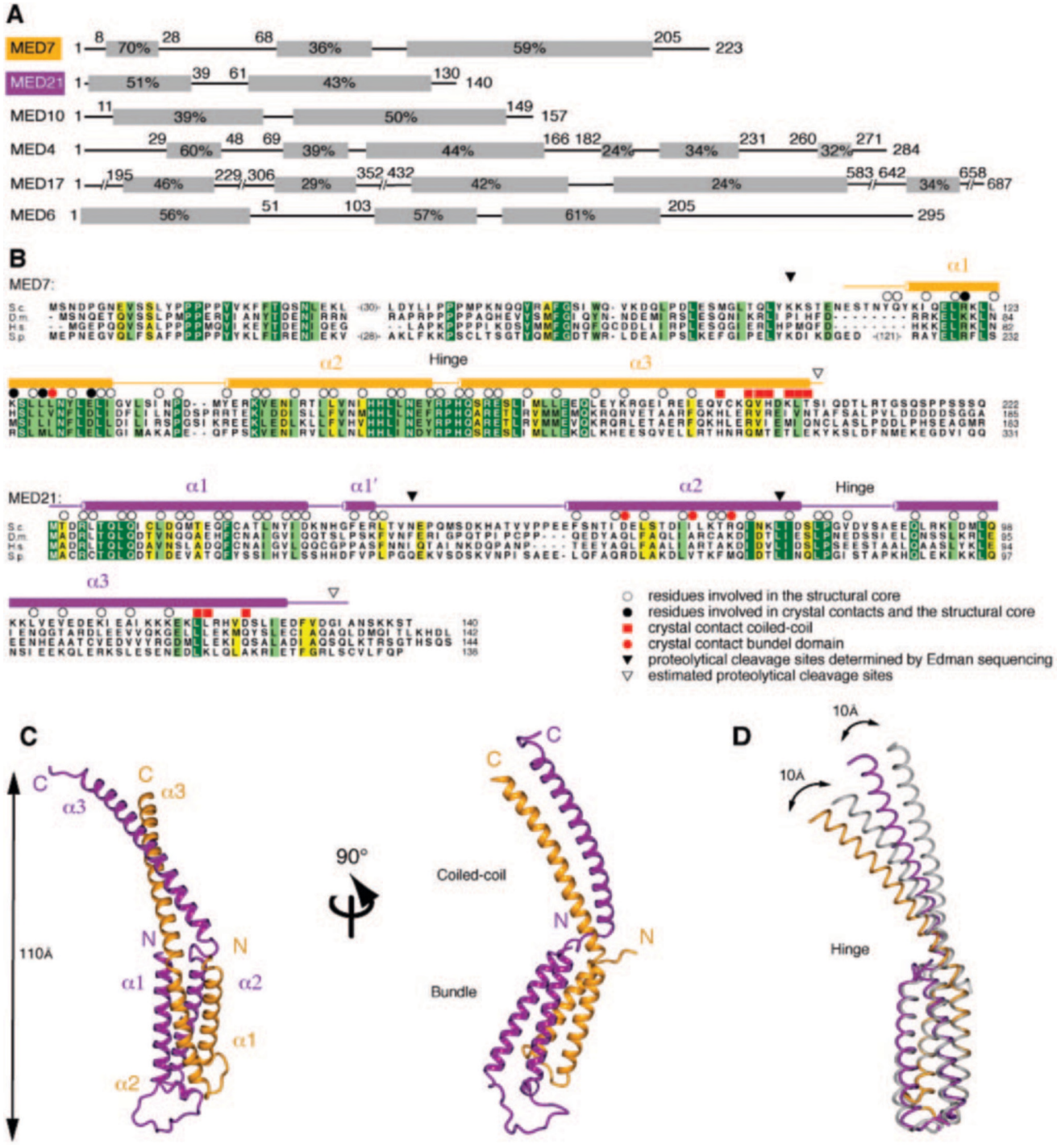

FIG. 1. **MED7·MED21 (Med7·Srb7) structure.** *A*, schematic diagrams of selected *S. cerevisiae* Mediator subunits. *Gray bars* indicate regions of sequence homology with the percentage sequence homology between yeast and human. *B*, sequence alignments of MED7 and MED21 from *S. cerevisiae* (*S.c.*), *Drosophila melanogaster* (*D.m.*), *Homo sapiens* (*H.s.*), and *Schizosaccharomyces pombe* (*S.p.*). Helical regions are shown *above* the alignments as *cylinders*. Residues are *highlighted* in *dark green*, *light green*, and *yellow* according to decreasing degree of conservation. Residues in the structural core are marked with *black open circles*. Core residues that are additionally involved in crystal contacts are marked with a *black dot*. *Red dots* and *squares* indicate residues involved in crystal contacts of the bundle and coiled-coil domains, respectively. *Filled triangles* indicate protease cleavage sites determined by Edman sequencing, and *outlined triangles* indicate approximate C-terminal protease cleavage sites. *C*, two views of a ribbon model of the MED7·MED21 complex, related by a 90° rotation around the vertical axis. MED7 is in *orange*, and MED21 is in *purple*. *D*, MED7·MED21 hinge. Structures in two different crystal forms have been superimposed with their bundle domains, resulting in a 10-Å difference at the end of the coiled-coil in the $C222_1$ crystal form (*color*) compared with the $P4_322$ crystal form (*gray*). The figures were prepared with DINO (www.dino3d.org).

group $C222_1$) by molecular replacement. We refined this structure to a free R-factor of 31.4% with data extending to 3.3 Å of resolution (Table I).

Elongated Two-domain Structure—MED7 and MED21 form a very elongated heterodimer of purely helical structure (Fig. 1*C*). The heterodimer extends over 110 Å, corresponding to ⅓ of the Mediator length (21) and amounting almost to the diameter of Pol II (39) (Fig. 1*C*). This elongated shape is consistent with an unusually short retention in size exclusion chromatography (Fig. 2). The retention of the MED7·MED21

TABLE I
Diffraction data and refinement statistics

r.m.s.d., root mean square deviation.

Crystal	Selenomethionine MAD MED7ΔNΔC/MED21ΔC[a]			Native MED7ΔNΔC/ MED21ΔC[a]	Native MED7ΔNΔC/ MED21
Data collection					
Space group	$P4_322$			$P4_322$	$C222_1$
a (Å)	85.6			85.7	121.5
b (Å)	85.6			85.7	128.9
c (Å)	185.2			183.0	170.2
Wavelength (Å)	0.9795 peak	0.9797 inflection	0.9686 remote	0.9795	1.0749
Resolution range	20-3.6 (3.73-3.6)[b]	20-3.6 (3.73-3.6)	20-3.6 (3.73-3.6)	50-3.0 (3.11-3.0)	50-3.3 (3.42-3.3)
Completeness (%)	100 (100)	100 (100)	100 (100)	98.6 (100)	99.6 (99.5)
Unique reflections	8,517	8,517	8,517	14,180	20,641
Redundancy	6.9	6.5	6.7	5.4	4.8
R_{sym}(%)	8.3 (21.0)	8.7 (32.0)	7.8 (26.0)	6.5 (26.2)	5.8 (36.2)
$\langle I/\sigma I \rangle$	7.6	6.4	6.8	8.9	10.4
f'	−8.0	−9.8	−3.8		
f''	4.9	2.5	3.7		
Refinement					
Number of residues				209	428
Non-hydrogen atoms				1,737	3,549
r.m.s.d. bonds (Å)				0.008	0.009
r.m.s.d. angles (°)[c]				1.164	1.37
Ramachandran plot (core/allowed/ additionally allowed)				94.3/5.7/0	87.9/11.8/0.3
R_{cryst}(%)				25.7	27.9
R_{free} (%)				28.9	31.4

[a] The triple point mutant L5M/L119M/L125M of MED21 was used.
[b] The numbers in parenthesis correspond to the highest resolution shell.
[c] PROCHECK (53).

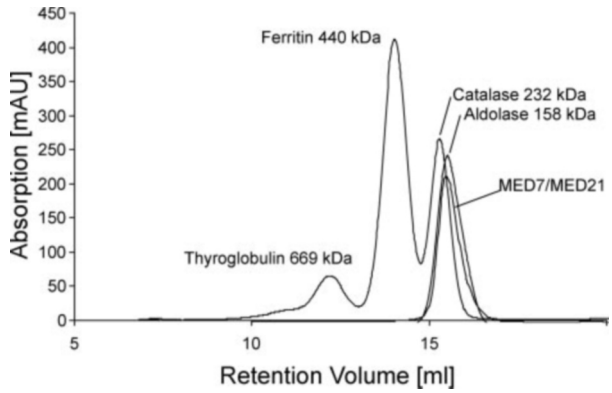

FIG. 2. **Size exclusion chromatography.** The MED7·MED21 complex shows an unusually short retention in size exclusion chromatography. The elution profile of MED7·MED21 on a Superose-6 column (Amersham Biosciences) is overlaid to those of standard proteins (thyroglobulin, ferritin, catalase, and aldolase). Protein elution was monitored by UV absorption at 280 nm. For details see "Experimental Procedures." *mAU*, milliabsorbance units.

species lies between that of the standard proteins aldolase (157 kDa) and catalase (230 kDa) and may be explained by formation of tetramers (dimers of heterodimers). Two different types of tetramers are observed in the crystal (Fig. 3, *C–D*), which show a computed (40) Stokes radius of 42–44 Å. This is in good agreement with the Stokes radii for aldolase and catalase (47 and 49 Å, respectively), whereas the Stokes radius of the MED7·MED21 heterodimer is only 31 Å. Thus, the complex apparently forms stable tetramers in solution. Dynamic light scattering also indicates a molecular weight well above that of the heterodimer, but the data quality did not allow for quantification.

MED7 and MED21 show no sequence similarity, but they have the same structural organization, comprising three extended helices. MED7 and MED21 tightly pack against each other, forming a heterodimer with two domains. A 4-helix bundle domain is formed by the two N-terminal α-helices of each subunit, and the C-terminal helices of the two subunits form a long coiled-coil protrusion (Fig. 1*C*). A "hinge" region connects the bundle domain to the coiled-coil protrusion.

A Conserved Flexible Hinge—Comparison of the MED7·MED21 structure in the two crystal forms reveals that the coiled-coil protrusion can undergo a hinge movement with respect to the bundle domain, giving rise to a 10-Å displacement of the C-terminal end of the protrusion (Fig. 1*D*). This repositioning of the protrusion is accommodated by a slight conformational adjustment in the hinge region. Thus, the MED7·MED21 heterodimer has an intrinsic flexibility that allows for a relative repositioning of the two domains. This flexibility is not due to the short C-terminal truncation of MED21 in the $C222_1$ crystal form since the two chemically identical heterodimers in the asymmetric unit also show two different conformations indicating the same hinge motion and since the truncated residues are not involved in packing interactions in the $C222_1$ crystal form. The high sequence conservation of amino acid residues in the hinge region of MED7 and MED21 (Fig. 1*B*) strongly suggests that the observed flexibility is functionally significant. A hinge movement is also predicted by molecular dynamics simulation with the Dynamite server (dynamite.biop.ox.ac.uk/dynamite).

MED7-MED21 Interaction—MED7 and MED21 form a continuous hydrophobic interface, which explains why subunits that are individually expressed in *E. coli* are structurally unstable and either poorly soluble or easily degraded. The hydrophobic residues in the MED7-MED21 interface along the coiled-coil protrusion are mostly conserved throughout eukaryotes and show a spacing typical for coiled coils (MED7 residues Leu-175, Leu-178, Leu-182, Ile-189, Ile-192; MED21 residues Ile-94, Leu-97, Leu-101, Val-104, Ala-111) (Figs. 1*B* and 2). In MED7 the regular spacing of the hydrophobic residues is discontinued only at residue Lys-185. The regular pattern in MED21 is similar, except for residues Gln-90, Lys-K108, and Lys-115, which, however, also participate in fold-stabilizing interactions. The conserved MED21 residue Gln-90 forms hydrogen bonds with Glu-172 and Arg-171 of MED7 and may contribute to the specificity of the heterodimeric interac-

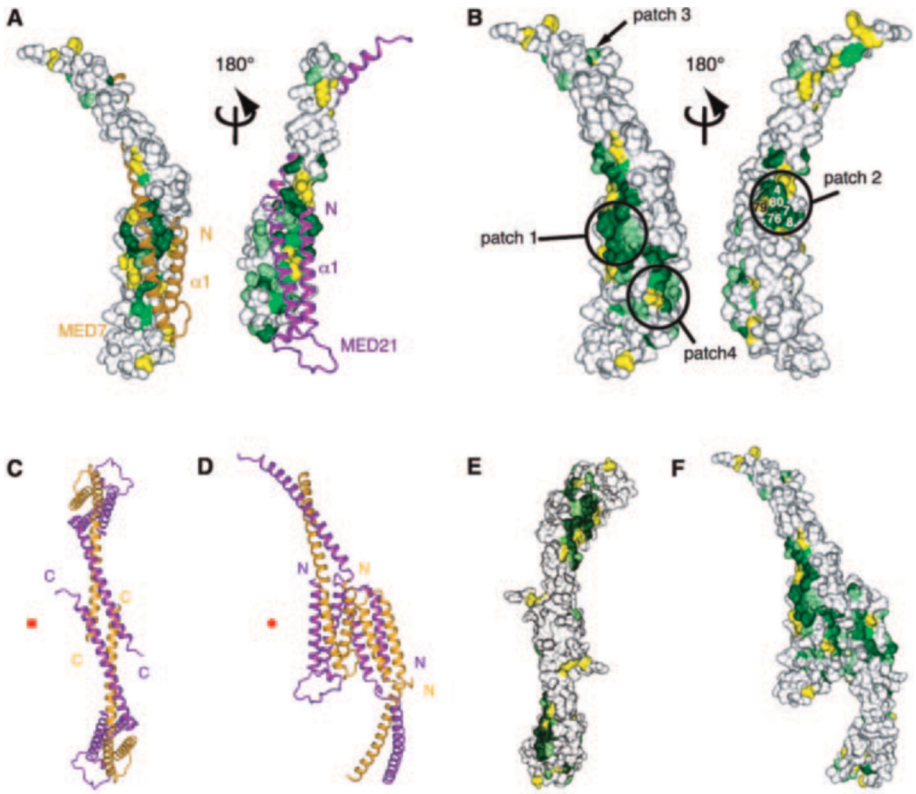

FIG. 3. **Interaction surfaces.** *A*, MED7-MED21 interactions. On the *left*, the Connelly surface of MED21 (probe radius 1.2 Å) is shown together with a ribbon model of MED7. The view is as in Fig. 1*C*. On the *right*, the Connelly surface of MED7 is shown together with a ribbon model of MED21. The two views are related by a 180° rotation around a vertical axis. Residues are highlighted in *dark green*, *light green*, and *yellow*, according to decreasing degree of conservation (compare Fig. 1*B*). *B*, conserved surface patches on the MED7·MED21 complex. The views are as in *A*. Four conserved surface patches are indicated. *C*, heterotetramerization in the crystal mediated by interaction of the open ends of the C-terminal coiled-coils. Residues involved in crystal contacts are marked in Fig. 1*B*. *D*, heterotetramerization in the crystal, mediated by interaction between the bundle domains. *E*, surface representation of the model in *C*. *F*, surface representation of the model in *D*.

tion. Given the high degree of sequence conservation of the crystallized regions, the MED7·MED21 structure must essentially be the same in all species. This conservation in structure explains why a chimeric MED21 protein consisting of the two human N-terminal helices (corresponding to yeast residues 1–81) and the yeast C-terminal helix (residues 82–140) is functional *in vivo* (41) and why truncation of the MED21-interacting region of MED7 is lethal in *Caenorhabditis elegans* (42).

A Unique Leucine Zipper—The coiled-coil protrusion resembles a canonical leucine zipper as it occurs in transcription factors like c-Jun (43) or Gcn4 (44, 45). The two helices of the coiled-coil separate at their C-terminal end. The inner side of this open end of the zipper is conserved and hydrophobic (MED21 residues Leu-118, Val-122, Ile-126, and Phe-129; MED7 residues Leu-203 and Val-199) and, thus, chemically different from the corresponding region in leucine zipper-containing transcription factors, which show exposed polar or charged residues for DNA binding in this region. Instead of binding DNA, the open end of the MED7·MED21 coiled-coil may interact with other Mediator subunits. In the crystal two heterodimers pack against each other via their coiled-coil ends (Fig. 3*C*), indicating that the open end of the coiled-coil may allow for protein interactions.

Conserved Interactions within the Middle Module—To map direct protein-protein interactions of the MED7·MED21 complex with other subunits in the Mediator middle module, we tested for copurification of subunits after their coexpression in *E. coli* (Fig. 4*A*). Such copurification can successfully map strong and specific direct protein-protein interactions, as demonstrated in our structure determination of the MED7·MED21 complex. The copurification assay is very stringent, because many different nonspecific competitor proteins are present in the *E. coli* lysate, because the stoichiometry of the complexes can be estimated with Coomassie-stained gels, and because the protein-protein complexes must persist over several copurification steps even when elevated salt concentrations of 600 mM NaCl are used. *E. coli* was cotransformed with two plasmids, a bicistronic plasmid expressing the MED7·MED21 heterodimer and a second plasmid with a different antibiotic resistance, expressing a third subunit. We found that the MED7·MED21 heterodimer strongly binds MED10 and MED4, which show 39 and 33% sequence homology between yeast and human, respectively, and are the most conserved core Mediator subunits aside from MED7, MED21, MED31 (Soh1), and MED6 (Fig. 4*A*). In contrast, the other two subunits of the middle module, MED1 or MED9, do not copurify with the MED7·MED21 complex. To test if MED21 alone is sufficient for the interactions with MED10 or MED4, we constructed bicistronic vectors for coexpression. These experiments revealed that MED21 alone is capable of binding MED10 or MED4 (Fig. 4*B*).

MED6 Bridges the Two Mediator Core Modules—We could additionally demonstrate that the MED7·MED21 heterodimer binds directly to MED6, which shows 34% sequence homology between yeast and human (Fig. 4*C*). Although MED7, MED21, MED4, and MED10 are all subunits of the middle module, MED6 is an integral part of the head module (46), suggesting that MED6 bridges between these two modules. To test if MED6 binds directly to MED17 (Srb4), the architectural subunit of the head module (47), we tagged MED6 with a C-terminal hexahistidine tag (*His*), fused MED17 to a N-terminal GST tag, and coexpressed the two subunits from a bicistronic vector. We could copurify the two subunits in two subsequent affinity chromatography steps using a Ni-NTA and a glutathione column (Fig. 4*C*). Successful purification of the complex was independent of the order of the affinity columns. The weakly conserved N-terminal part of MED17 and the nonconserved C-terminal part of MED6 are not required for binding since truncated variants of MED17 (residues 241–688) and MED6 (residues 1–214) were sufficient for the interaction. Our results are consistent with a functional interaction between MED17 and MED6 observed previously (46). The results are further consistent with a very recent study of Mediator subunit

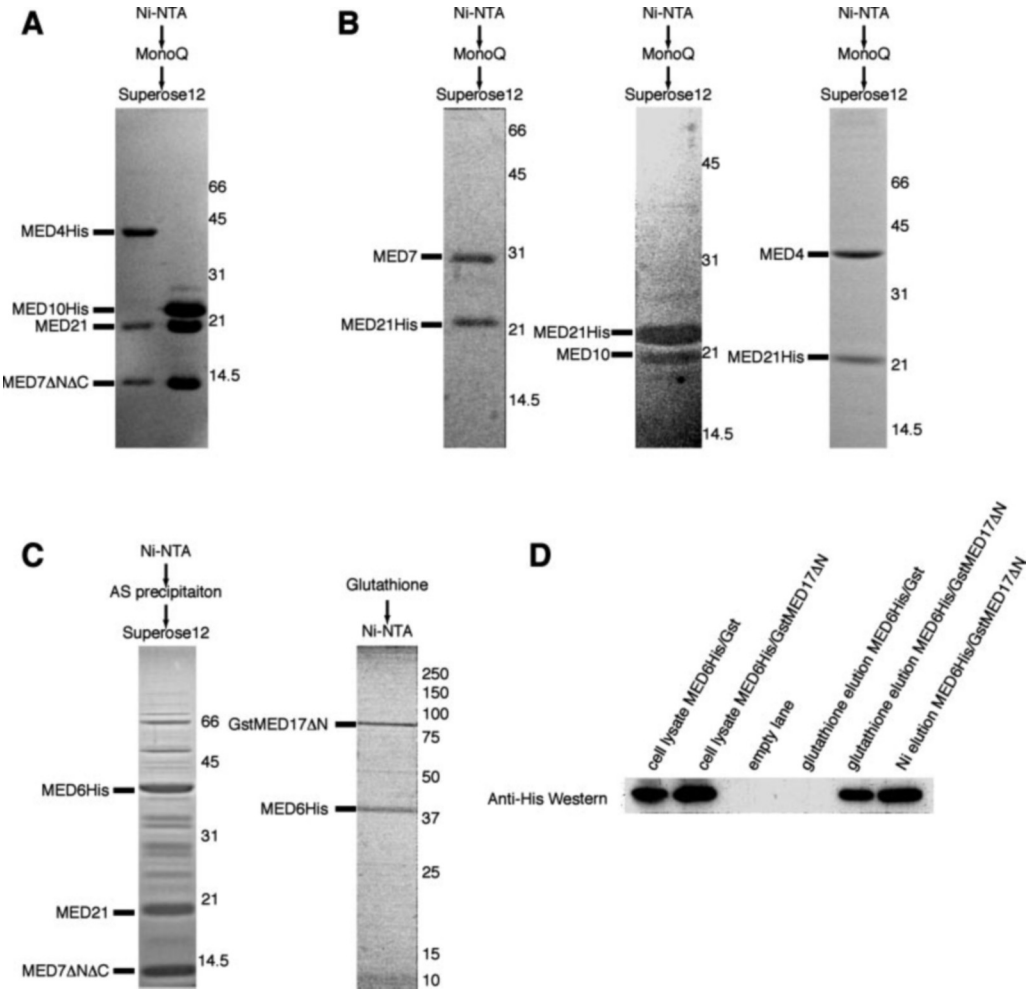

FIG. 4. **Protein-protein interactions of the MED7·MED21 complex.** *A*, copurification of MED7ΔNΔC·MED21 heterodimer with MED10His and MED4His. *B*, copurification of MED21His with MED7, MED10 and MED4. *C*, copurification of MED6His with MED7ΔNΔC·MED21 or GSTMED17ΔN. A schematic presentation of the purification procedure is shown *above* the *gels*. Gels in *A–C* were stained with Coomassie Blue. *AS*, ammonium sulfate. *D*, Western blot of the GSTMED17ΔN·MED6His purification. The binding of MED6 to MED17 is not due to the presence of the GST tag since a purification using GST only does not yield MED6 (*fourth lane*).

interactions by yeast two-hybrid analysis (48). In conclusion, MED6 physically bridges between the two Mediator core modules, interacting with MED17 in the head module and with the MED7·MED21 heterodimer in the middle module.

DISCUSSION

Conserved Mediator Core Architecture—Our data show that the MED7·MED21 heterodimer tightly binds to other highly conserved Mediator subunits via its evolutionarily conserved regions and, thus, plays a central architectural role within Mediator. Our findings are consistent with published data on Mediator subunit interactions, which stem from coexpression of subunits in insect cells (23), coimmunoprecipitation (46), the split ubiquitin assay (49), and from yeast two-hybrid analysis (50). These studies additionally showed that the remaining subunits of the middle module, MED1 and MED9, are both bound by MED7, and MED1 is also bound by MED4. Because we did not detect MED1-MED7 or MED9-MED7 interaction with the N-terminally truncated MED7 variant, this indicates that MED1 and MED9 bind to the MED7 N-terminal region. Taken together, these results establish the MED7·MED21 complex as the conserved assembly scaffold of the middle module (Fig. 5). Sequence-based predictions of secondary structure (51) and coiled-coils (52) strongly suggest that subunits MED10 and MED4 are largely helical and form coiled-coils that may mediate the strong subunit interactions observed here and may span large distances on the Pol II surface.

Analysis of the molecular surface of the MED7·MED21 heterodimer reveals that the majority of the surface is hydrophobic, consistent with the observed extended interactions with other subunits. Four conserved surface patches (Fig. 3*B*) may serve as protein interaction sites and befit the architectural role of the MED7·MED21 heterodimer. Patch 1 and 2 are near the hinge region. Patch 2 includes the highly conserved N-terminal helix α1 of MED21 (residues Arg-4, Gln-7, Leu-8) and a part of MED21 helix α2 (residues Leu-76, Ser-79, Leu-80, Fig. 3). Because the highly conserved 7 N-terminal MED21 residues are required for MED6 binding (49), we propose that patch 2 constitutes the MED6 binding site. Patches 1, 3, and 4 may bind to subunits of the middle module but may also be involved in interactions with Pol II. Patches 3 and 4 are involved in crystal contacts. Patch 3 corresponds to the open end of the coiled-coil that stacks against a neighboring coiled-coil in the crystal (Fig. 3*C*), and patch 4 mediates dimerization of bundle domains of neighboring MED7·MED21 heterodimers in the crystal (Fig. 3*D*). The resulting two types of tetramers in the crystal do not show additional conserved surface patches (Fig. 3, *E–F*). Taken together, the high conservation of the MED7·MED21 heterodimer, its many interactions with conserved subunits,

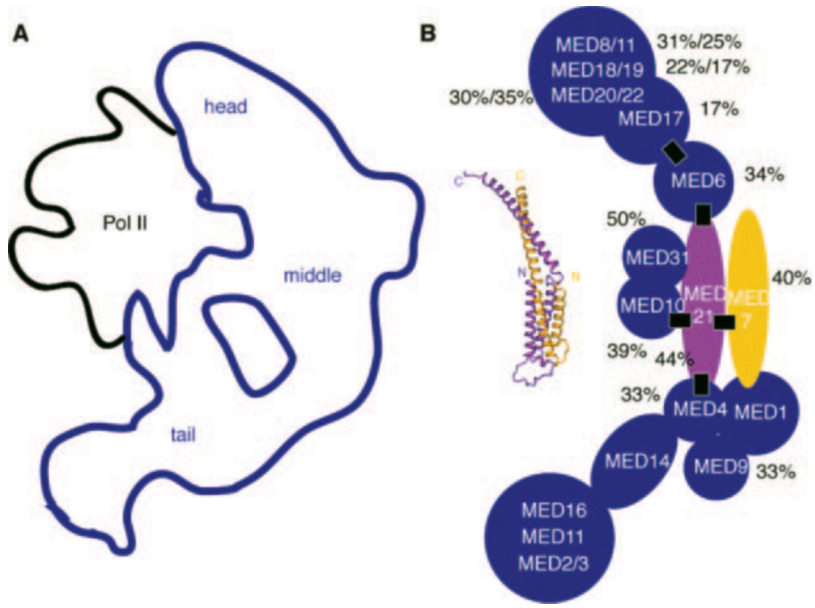

FIG. 5. **Mediator architecture.** *A*, outline of Mediator bound to Pol II according to electron microscopy (21). The suggested head, middle, and tail modules are indicated. *B*, Mediator subunit architecture. All depicted subunits are at least partially conserved throughout eukaryotes, except MED2 and MED3. The percentage of sequence homology between yeast and human subunits is indicated for the well conserved Mediator subunits. The four-subunit kinase module and the putative Mediator subunit MED5 have been omitted. For size comparison, the structure of the MED7·MED21 complex and the Pol II-Mediator complex in *A* are drawn to scale. *Black rectangles* indicate direct protein-protein interactions detected in this study.

and its extended conserved hydrophobic surface patches all indicate that the structural architecture of the central region of the core Mediator is the same in all species.

Conserved Hinges and Mediator Function—Electron microscopy of free yeast Mediator and Mediator bound to Pol II revealed a dramatic structural rearrangement (20, 21). Whereas free Mediator is relatively compact, it becomes extended upon Pol II binding and is wrapped around the polymerase surface in the Pol II-Mediator complex (Fig. 5*A*). This transition apparently involves a large change in the relative position of the Mediator middle and head modules (21). Our data suggest that the MED6 subunit plays a central role in this process because it bridges between the two modules of the core Mediator. Secondary structure prediction for MED6 reveals extended loop regions and helices with low probability (51), indicating a strong intrinsic flexibility for MED6. MED6 may form a conserved flexible connection between the head and middle modules. The bridging role of MED6 is relevant for Mediator function *in vivo*. A point mutation in MED17 suppresses temperature-sensitive mutations in the N-terminal region of MED6 that weaken the interaction with MED17 (54). The interaction of MED21 with MED6 is apparently essential *in vivo*, as a deletion mutant of yeast lacking the 15 N-terminal residues of MED21 is not viable (31).

Strong structural changes have also been observed in the mammalian Mediator coactivators CRSP and ARC upon binding of activator proteins (22, 38). In addition to the MED6 hinge, the intrinsic flexibility of the MED7·MED21 heterodimer may account for these conformational changes. The hinge region between the two domains of the heterodimer may allow for flexibility within the middle module, because the relative locations of subunits bound to surface patch 3 on the coiled-coil and patches 1, 2, and 4 on the bundle domain can change. Binding of MED6 to the hinge region of the MED7·MED21 heterodimer may restrict or coordinate hinge motions. The repositioning of different parts of the core Mediator, enabled by conserved hinges as suggested here and triggered by the interaction with various partners, may be crucial for Mediator function.

Acknowledgments—We thank A. Meinhart for help with structure determination and C. Buchen for help with protein interaction studies. Part of this work was performed at the Swiss Light Source, Paul Scherrer Institut, Villigen, Switzerland. We thank C. Schulze-Briese and co-workers for help.

REFERENCES

1. Naar, A. M., Lemon, B. D., and Tjian, R. (2001) *Annu. Rev. Biochem.* **70,** 475–501
2. Myers, L. C., and Kornberg, R. D. (2000) *Annu. Rev. Biochem.* **69,** 729–749
3. Malik, S., and Roeder, R. G. (2000) *Trends Biochem. Sci.* **25,** 277–283
4. Bjorklund, S., and Gustafsson, C. M. (2004) *Adv. Protein Chem.* **67,** 43–65
5. Flanagan, P. M., Kelleher, R. J., III, Sayre, M. H., Tschochner, H., and Kornberg, R. D. (1991) *Nature* **350,** 436–438
6. Kim, Y. J., Bjorklund, S., Li, Y., Sayre, M. H., and Kornberg, R. D. (1994) *Cell* **77,** 599–608
7. Kelleher, I., R. J., Flanagan, P. M., and Kornberg, R. D. (1990) *Cell* **61,** 1209–1215
8. Holstege, F. C. P., Jennings, E. G., Wyrick, J. J., Lee, T. I., Hengartner, C. J., Green, M. R., Golub, T. R., Lander, E. S., and Young, R. A. (1998) *Cell* **95,** 717–728
9. Mittler, G., Kremmer, E., Timmers, H. T., and Meisterernst, M. (2001) *EMBO Rep* **2,** 808–813
10. Baek, H. J., Malik, S., Qin, J., and Roeder, R. G. (2002) *Mol. Cell. Biol.* **22,** 2842–2852
11. Bourbon, H. M., Aguilera, A., Ansari, A. Z., Asturias, F. J., Berk, A. J., Bjorklund, S., Blackwell, T. K., Borggrefe, T., Carey, M., Carlson, M., Conaway, J. W., Conaway, R. C., Emmons, S. W., Fondell, J. D., Freedman, L. P., Fukasawa, T., Gustafsson, C. M., Han, M., He, X., Herman, P. K., Hinnebusch, A. G., Holmberg, S., Holstege, F. C., Jaehning, J. A., Kim, Y. J., Kuras, L., Leutz, A., Lis, J. T., Meisterernest, M., Naar, A. M., Nasmyth, K., Parvin, J. D., Ptashne, M., Reinberg, D., Ronne, H., Sadowski, I., Sakurai, H., Sipiczki, M., Sternberg, P. W., Stillman, D. J., Strich, R., Struhl, K., Svejstrup, J. Q., Tuck, S., Winston, F., Roeder, R. G., and Kornberg, R. D. (2004) *Mol. Cell* **14,** 553–557
12. Boube, M., Joulia, L., Cribbs, D. L., and Bourbon, H. M. (2002) *Cell* **110,** 143–151
13. Nonet, M. L., and Young, R. A. (1989) *Genetics* **123,** 715–725
14. Thompson, C. M., Koleske, A. J., Chao, D. M., and Young, R. A. (1993) *Cell* **73,** 1361–1375
15. Cantin, G. T., Stevens, J. L., and Berk, A. J. (2003) *Proc. Natl. Acad. Sci. U. S. A.* **100,** 12003–12008
16. Cosma, M. P., Panizza, S., and Nasmyth, K. (2001) *Mol. Cell* **7,** 1213–1220
17. Liu, Y., Ranish, J. A., Aebersold, R., and Hahn, S. (2001) *J. Biol. Chem.* **276,** 7169–7175
18. Yudkovsky, N., Ranish, J. A., and Hahn, S. (2000) *Nature* **408,** 225–229
19. Naar, A. M., Taatjes, D. J., Zhai, W., Nogales, E., and Tjian, R. (2002) *Genes Dev.* **16,** 1339–1344
20. Asturias, F. J., Jiang, Y. W., Myers, L. C., Gustafsson, C. M., and Kornberg, R. D. (1999) *Science* **283,** 985–987
21. Davis, J. A., Takagi, Y., Kornberg, R. D., and Asturias, F. A. (2002) *Mol. Cell* **10,** 409–415
22. Taatjes, D. J., Naar, A. M., Andel, F., III, Nogales, E., and Tjian, R. (2002) *Science* **295,** 1058–1062
23. Kang, J. S., Kim, S. H., Hwang, M. S., Han, S. J., Lee, Y. C., and Kim, Y. J. (2001) *J. Biol. Chem.* **276,** 42003–42010
24. Dotson, M. R., Yuan, C. X., Roeder, R. G., Myers, L. C., Gustafsson, C. M., Jiang, Y. W., Li, Y., Kornberg, R. D., and Asturias, F. J. (2000) *Proc. Natl. Acad. Sci. U. S. A.* **97,** 14307–14310
25. Linder, T., and Gustafsson, C. M. (2004) *J. Biol. Chem.* **279,** 49455–49459
26. Myers, L. C., Gustafsson, C. M., Bushnell, D. A., Lui, M., Erdjument-Bromage, H., Tempst, P., and Kornberg, R. D. (1998) *Genes Dev.* **12,** 45–54
27. Hengartner, C. J., Thompson, C. M., Zhang, J., Chao, D. M., Liao, S. M., Koleske, A. J., Okamura, S., and Young, R. A. (1995) *Genes Dev.* **9,** 897–910
28. Tudor, M., Murray, P. J., Onufryk, C., Jaenisch, R., and Young, R. A. (1999) *Genes Dev.* **13,** 2365–2368

29. Lutzmann, M., Kunze, R., Buerer, A., Aebi, U., and Hurt, E. (2002) *EMBO J.* **21,** 387–397
30. Posas, F., Wurgler-Murphy, S. M., Maeda, T., Witten, E. A., Thai, T. C., and Saito, H. (1996) *Cell* **86,** 865–875
31. Gromoller, A., and Lehming, N. (2000) *FEBS Lett.* **484,** 48–54
32. Meinhart, A., Blobel, J., and Cramer, P. (2003) *J. Biol. Chem.* **278,** 48267–48274
33. Otwinowski, Z., and Minor, W. (1996) *Methods Enzymol.* **276,** 307–326
34. Terwilliger, T. C. (2002) *Acta Crystallogr. D Biol. Crystallogr.* **58,** 1937–1940
35. La Fortelle, E. D., and Bricogne, G. (1997) *Methods Enzymol.* **276,** 472–494
36. Jones, T. A., Zou, J. Y., Cowan, S. W., and Kjeldgaard, M. (1991) *Acta Crystallogr. A* **47,** 110–119
37. Brunger, A. T., Adams, P. D., Clore, G. M., DeLano, W. L., Gros, P., Grosse-Kunstleve, R. W., Jiang, J. S., Kuszewski, J., Nilges, M., Pannu, N. S., Read, R. J., Rice, L. M., Simonson, T., and Warren, G. L. (1998) *Acta Crystallogr. D Biol. Crystallogr.* **54,** 905–921
38. Taatjes, D. J., Schneider-Poetsch, T., and Tjian, R. (2004) *Nat. Struct. Mol. Biol.* **11,** 664–671
39. Cramer, P., Bushnell, D. A., and Kornberg, R. D. (2001) *Science* **292,** 1863–1876
40. Garcia De La Torre, J., Huertas, M. L., and Carrasco, B. (2000) *Biophys. J.* **78,** 719–730
41. Chao, D. M., Gadbois, E. L., Murray, P. J., Anderson, S. F., Sonu, M. S., Parvin, J. D., and Young, R. A. (1996) *Nature* **380,** 82–85
42. Kwon, J. Y., Kim-Ha, J., Lee, B. J., and Lee, J. (2001) *FEBS Lett.* **508,** 305–308
43. Junius, F. K., O'Donoghue, S. I., Nilges, M., Weiss, A. S., and King, G. F. (1996) *J. Biol. Chem.* **271,** 13663–13667
44. Keller, W., Konig, P., and Richmond, T. J. (1995) *J. Mol. Biol.* **254,** 657–667
45. Holm, L., and Sander, C. (1995) *Trends Biochem. Sci.* **20,** 478–480
46. Lee, Y. C., and Kim, Y. J. (1998) *Mol. Cell. Biol.* **18,** 5364–5370
47. Koh, S. S., Ansari, A. Z., Ptashne, M., and Young, R. A. (1998) *Mol. Cell* **1,** 895–904
48. Guglielmi, B., van Berkum, N. L., Klapholz, B., Bijma, T., Boube, M., Boschiero, C., Bourbon, H. M., Holstege, F. C., and Werner, M. (2004) *Nucleic Acids Res.* **32,** 5379–5391
49. Gromoller, A., and Lehming, N. (2000) *EMBO J.* **19,** 6845–6852
50. Uetz, P., Giot, L., Cagney, G., Mansfield, T. A., Judson, R. S., Knight, J. R., Lockshon, D., Narayan, V., Srinivasan, M., Pochart, P., Qureshi-Emili, A., Li, Y., Godwin, B., Conover, D., Kalbfleisch, T., Vijayadamodar, G., Yang, M., Johnston, M., Fields, S., and Rothberg, J. M. (2000) *Nature* **403,** 623–627
51. Rost, B. (1996) *Methods Enzymol.* **266,** 525–539
52. Lupas, A., Van Dyke, M., and Stock, J. (1991) *Science* **252,** 1162–1164
53. Laskowski, R. A., MacArthur, M. W., Moss, D. S., and Thornton, J. M. (1993) *J. Appl. Crystallogr.* **26,** 283–291
54. Lee, Y. C., and Kim, Y. J. (1998) *Mol. Cell. Biol.* **18,** 5367–5370